Thermochimica Acta, 104 (1986) 13–29
Elsevier Science Publishers B.V., Amsterdam – Printed in The Netherlands

THERMAL RUNAWAY REACTIONS IN A LOW THERMAL INERTIA APPARATUS

J.C. LEUNG and H.K. FAUSKE

Fauske & Associates, Inc., Burr Ridge, Illinois 60521 (U.S.A.)

H.G. FISHER

Union Carbide Corporation, South Charleston, West Virginia 25303 (U.S.A.)

(Received 17 December 1985)

ABSTRACT

A new apparatus utilizing a unique low heat capacity sample container is described for studying thermal runaway reactions. Other features provided by this new technique include: nearly equal pressures between sample container and the outside containment vessel as the runaway proceeds, a nearly zero temperature gradient outside the sample container to minimize heat loss, a magnetic stirring mechanism, and a remote feed capability. Thermal data obtained for styrene polymerization and di-t-butyl peroxide decomposition were shown to be in excellent agreement with previously published kinetic models. Finally, a base-catalyzed phenol–formaldehyde reaction in a runaway situation is presented.

INTRODUCTION

Two devices commonly used to obtain information on the exothermicity of runaway reactions are the differential scanning calorimeter (DSC) [1] and the accelerating rate calorimeter (ARC™) [2]. A DSC can yield the heat of reaction data and some measure of the reaction rate, but it cannot readily produce pressure data. In addition, DSC data cannot be directly extrapolated to normal operating and upset conditions because these data are obtained at a fixed heating rate. Another drawback is the use of a very small ($\approx$ 10 mg) sample which may not be representative of the bulk mixture. Thus the DSC is of limited use in assessing emergency relief requirements.

The ARC apparatus overcomes most of these disadvantages. Numerous publications have appeared detailing the performance of the ARC in many important exothermic systems [3–5]. The ARC has a 10 cm^3 sample bomb and can follow the runaway reaction in an adiabatic manner. However, one of the major disadvantages of the ARC is the relatively high heat capacity of the sample bomb. A commonly calculated quantity is the so-called phi-factor, or thermal inertia, which is defined by eqn. (1)

$$\phi = \frac{m_s c_{vs} + m_b c_{vb}}{m_s c_{vs}} \tag{1}$$

0040-6031/86/$03.50

where m_s and m_b are the masses of the sample and container or "bomb", respectively, and c_{vs} and c_{vb} are the specific heats of the sample and container at constant volume, * respectively. Hence a ϕ-factor of 2.0 means that half of the reaction heat given off goes into sensible heat of the sample container. The total temperature rise would be only half of that in the adiabatic case ($\phi = 1.0$). Depending on the material of construction, the ϕ-factor of the ARC bomb typically varies between 2.0 and 6.0. Thus important exotherms at higher temperatures can be missed. Even though techniques have been suggested for recalculating the ARC data to a ϕ-factor of unity, these data cannot be safely extrapolated above the peak temperature of the raw data [6,7].

A low thermal inertia apparatus with a typical ϕ-factor of 1.05 has been developed as part of an extensive research and development program of AIChE's Design Institute for Emergency Relief Systems (DIERS). The capabilities of the apparatus include measurement of thermal data, flow regime characterization, and most important of all, determination of vent sizing data under nearly adiabatic runaway reaction conditions. This paper will only address the acquisition of thermal data since other aspects have been covered elsewhere [8].

EXPERIMENTAL

The key feature of the DIERS bench-scale apparatus is the use of a unique low thermal mass test cell design to reduce its heat capacity. The test cell has a volume of 120 cm^3 and a wall thickness of 0.13 mm and its weight including the glass-encapsulated magnetic stirrer is approximately 21 g yielding a typical ϕ-factor of about 1.05. This test cell is contained in a larger containment vessel as shown in Fig. 1. The weakness of the test cell is compensated by using a pressure equalization system such that the test cell is subjected to only a tolerable pressure difference with its environment. The containment vessel serves to prevent bursting of the test cell by regulating its own pressure to follow the test cell pressure during a runaway. The differential output between the test cell and containment pressure transducers (P_1 and P_2) is fed to a differential controller (API type 501 K $\pm$ 50 μA double set point meter relay). By using the set points on the controller to open and close appropriate solenoid valves, pressure changes (up to about 300 psi/s) are rapidly equilibrated.

A small heater coil weighing about 5 g is situated outside the test cell and this inner heater is used to increase the test sample to a temperature level

* If specific heat values at constant volume are not available, they can be approximated by the corresponding values at constant pressure.

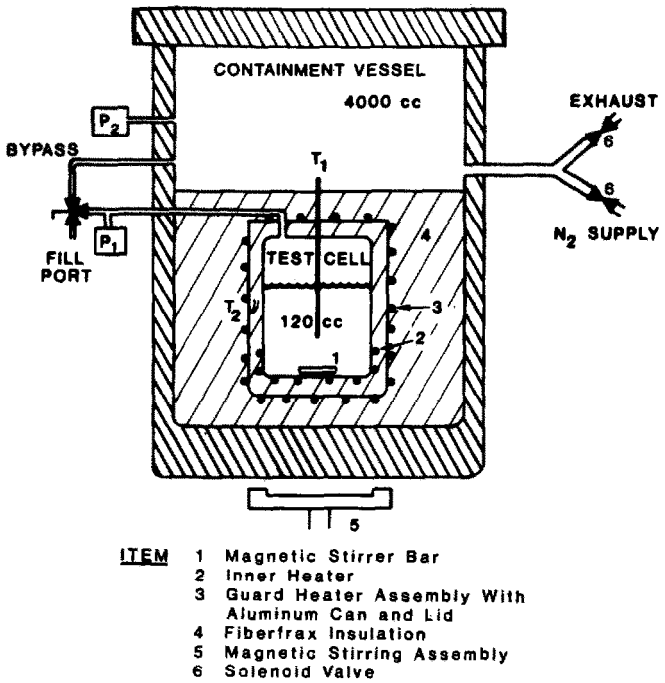

Fig. 1. Bench-scale test apparatus.

where a runaway exotherm can be detected. The outer guard heater coil is fastened onto the outside wall of an aluminum can and this can is separated from the test cell by a uniform layer (≈ 4 mm thick) of Fiberfrax insulation. Thus the aluminum can serves to provide a uniform temperature environment for the test cell and its content. A fast response thermocouple (T_2) is attached to the inside surface of the aluminum can and during a runaway the temperature in the aluminum can is regulated to follow the sample temperature (T_1) by supplying appropriate power to the guard heater. Thus heat loss to the environment is kept to a minimum.

The maximum heat rate from the guard heater is somewhat dependent on the temperature and pressure levels, but typically ranges from 50–100°C min^{-1}. For sample heat rates in excess of these values, the heat loss becomes relatively unimportant in relation to the rapid heat release. Heat loss has been calibrated with non-reacting fluids by measuring the temperature decay rate at elevated temperatures and pressures. A heat loss rate of less than 0.1°C min^{-1} can usually be achieved below 350°C and 350 psia.

A three-way valve and a bypass line arrangement as shown in Fig. 1 provides an added capability to evacuate the atmosphere inside the test cell prior to charging the sample at the fill port. In addition, catalysts or initiators can be charged separately after the sample has been brought up to the desired reacting temperature. For a detailed description of the DIERS bench-scale equipment see ref. 9.

RESULTS AND DISCUSSION

Styrene thermal polymerization

The thermal polymerization of styrene monomer, inhibited with 15 ppm t-butyl catechol, was studied using 80 g of a 80–20% by weight of a styrene–ethylbenzene solution. This yields a ϕ-factor of 1.05 in the present apparatus *. The pressure and temperature data obtained from this experiment are illustrated in Fig. 2. This figure shows that the exotherm was initiated at about 115°C after a few heat-wait-search periods (not shown) and that the heat evolved caused the temperature and pressure of the sample to increase to 343°C and 300 psia (with air pad), respectively. Figure 3 indicates that the self-heat rate started at about 0.3°C min^{-1} during onset and reached a peak rate of about 25°C min^{-1} at 270°C. Pressure build-up is an important parameter associated with runaway reactions; Figs. 4 and 5 illustrate two possible forms in which the pressure data are commonly presented.

For a single reaction system, the following heat balance equation [10] relates the incremental temperature change to the change in conversion for adiabatic operation.

$$m_t \phi c_v \, dT = -\Delta H_r m \, dx \tag{2}$$

where, m_t = total mass of reacting mixture, m = mass of limiting reactant corresponding to zero conversion, c_v = specific heat of mixture at constant volume, ΔH_r = heat of reaction per unit mass of limiting reactant (keeping

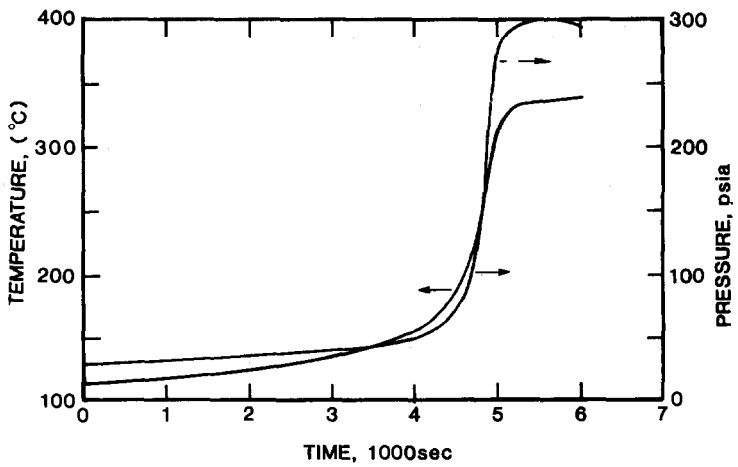

Fig. 2. Temperature and pressure behavior during a styrene runaway polymerization (64 g styrene, 16 g ethylbenzene, 20 g test cell with air atmosphere).

* ϕ-Factor is calculated based on the total sample, not on the monomer alone.

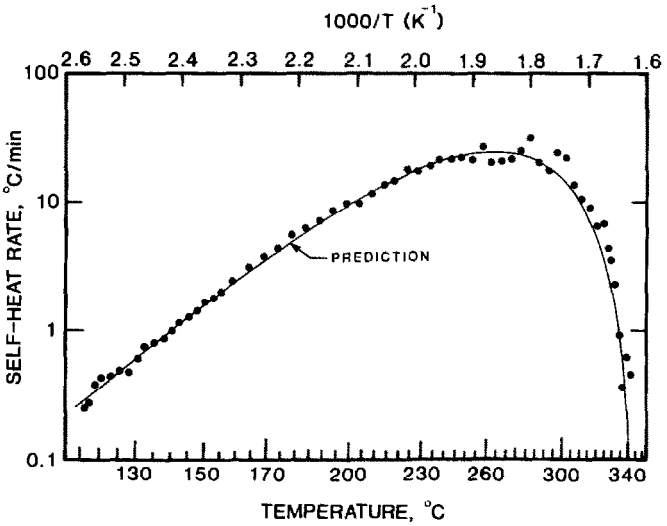

Fig. 3. Self-heat rate data from styrene runaway polymerization.

the convention that ΔH_r is negative for exothermic reaction) and $x =$ conversion in terms of limiting reactant. If c_v and ΔH_r are taken as constants, eqn. (2) can be immediately integrated to give the following relationship between temperature and conversion

$$T - T_0 = -\frac{\Delta H_r}{\phi c_v}\frac{m}{m_t}(x - x_0) \tag{3}$$

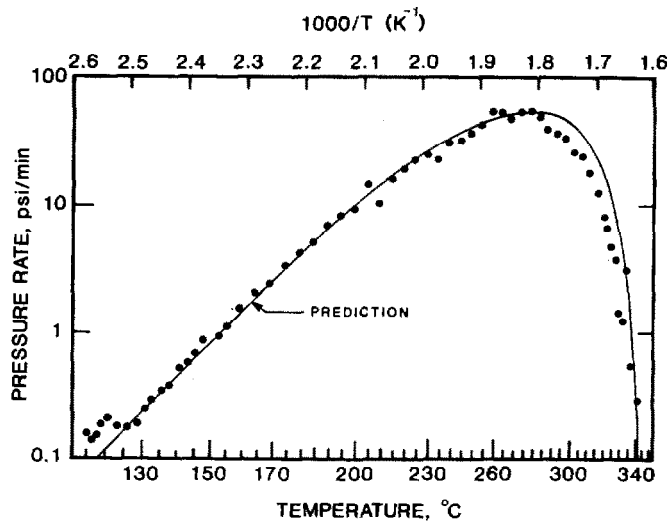

Fig. 4. Pressure rise rate data from styrene runaway polymerization.

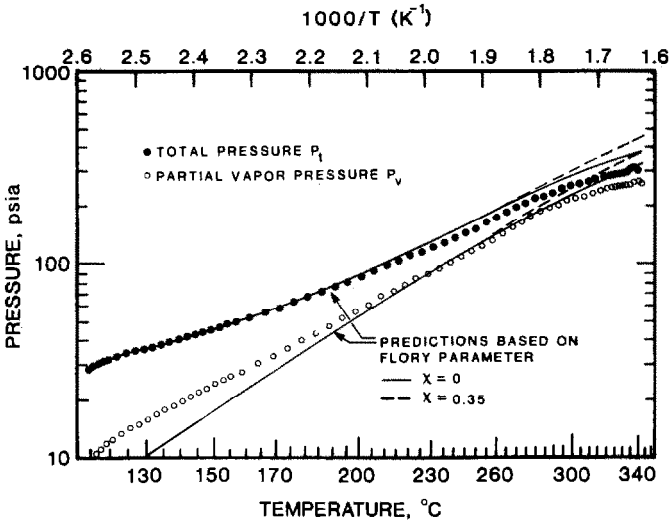

Fig. 5. Pressure–temperature data from styrene runaway polymerization.

When the reaction is completed, the above equation becomes

$$T_{max} - T_0 = -\frac{\Delta H_r}{\phi c_v}\frac{m}{m_t}(1 - x_0) \tag{4}$$

Assuming zero conversion at the onset temperature of T_0, eqn. (4) can be used to yield a quick estimate of the heat of polymerization based on the styrene test. Using an average specific heat value of 0.55 cal/g°C, * we have

$$\Delta H_r = -\frac{\phi c_v (T_{max} - T_0)}{(m/m_t)} = -\frac{(1.05)(0.55\ \text{cal/g°C})(343 - 115\text{°C})}{(0.8)}$$

$$= -164.5\ \text{cal/g styrene.}$$

This compares very well with the literature value of −173.4 cal/g at the mean reaction temperature of 227°C [11].

Consider for the moment that a simple first-order reaction can be written in the usual form (assuming a constant reacting mixture volume)

$$\frac{d(1-x)}{dt} = -k(1-x) \tag{5}$$

since the reactant mass fraction is equal to $1 - x$. Substituting eqns. (2) and (4) into eqn. (5) leads to the following expression relating the thermal measurable parameter, T, to the reaction rate constant [3]

$$k = \frac{dT/dt}{T_{max} - T} \tag{6}$$

* At 115°C, c_v for 80–20% styrene–ethylbenzene mixture is estimated to be 0.492 cal/g°C. At 343°C, c_v for 80–20% polystyrene–ethylbenzene solution is best estimated to be 0.608 cal/g°C (see Appendix), hence yielding an average c_v of 0.55 cal/g°C.

where k, the first-order reaction rate constant, has the units of reciprocal time. This reaction rate constant increases exponentially with temperature as in the Arrhenius expression

$$k = A \exp\left(-\frac{E_A}{RT}\right) \tag{7}$$

where A is the pre-exponential frequency factor, E_A is the activation energy of the reaction, and R is the gas constant. The plot of ln K vs. $1/T$ is, therefore, expected to be a straight line if indeed the reaction is first-order. The initial self-heat rate can be obtained from eqns. (2) and (4) to give

$$\ln\left(\frac{dT}{dt}\right)_0 = \ln(A\,\Delta T_{max}) - \frac{E_A}{R}\left(\frac{1}{T}\right) \tag{8}$$

which indicates that the initial slope of a plot of self-heat rate data (on logarithmic scale) vs. reciprocal temperature will yield the ratio E_A/R, and hence the activation energy.

Figure 6 is a plot of the first-order rate constant from the styrene runaway data. Obviously the data suggest that the reaction does not obey a simple first-order kinetic model. However, the initial data below 180°C can be correlated quite well with the initial polymerization rate equation obtained from ref. 12. At higher temperatures, and therefore higher conversion, the kinetic data exhibit a negative deviation from the Arrhenius type behavior, thus suggesting a higher than first-order kinetic model.

Hamielec et al. [13,14] have published a thermally initiated, free-radical polymerization kinetic model with gel effect to describe the styrene system. Their model is based on isothermal conversion data obtained in the tempera-

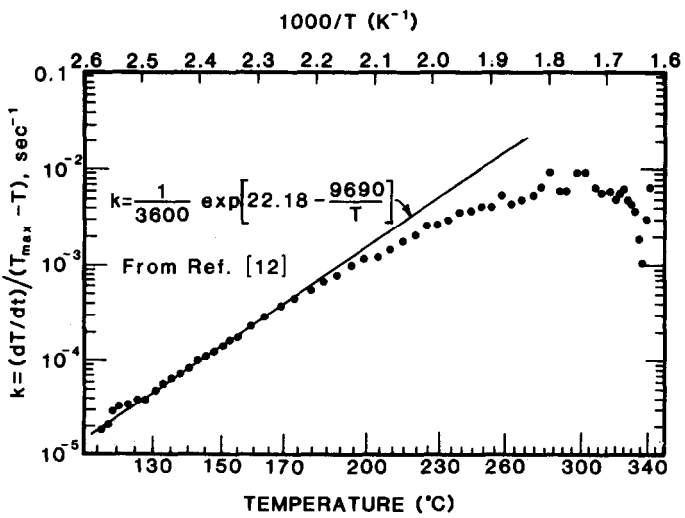

Fig. 6. First-order kinetic rate data from styrene runaway polymerization.

ture range of 100–200°C and was found to correlate their data up to 230°C [14]. This model was used to predict the behavior in the present runaway test. The temperature prediction is based on the differential heat balance of eqn. (2) together with the kinetic equations of ref. 13 and some detailed physical property data [6,15] outlined in the Appendix. Figures 3 and 4 illustrate the excellent agreement between this kinetic model and the present data. Our runaway data provide further validation of Hamielec's model above its original data base. The total temperature rise, which is a measure of the heat of polymerization, is also in good agreement with the expected value.

The pressure prediction accounts for the lowering in activity of both the monomer and the solvent in the presence of polymer. Activities, a_i, according to Flory and Huggins in ref. 16 are expressed in volume fractions, Φ, as

$$\ln a_i = \ln \Phi_i + (1 - 1/M_p)\Phi_p + \chi\Phi_p^2 \tag{9}$$

where M_p is the molecular weight of the polymer, χ is known as the Flory parameter, subscript i denotes either the styrene or ethylbenzene component, and Φ_p is the polymer volume fraction. In the present prediction, the polymer molecular weight effect in eqn. (9) can be ignored and the Flory parameter usually takes on a value between 0 and 0.5 [16]. The activity of the polymer is negligible and the volatile partial pressure can be predicted according to

$$P_v = \Sigma a_i P_i^0 \tag{10}$$

where P_i^0 is the pure component vapor pressure. The predicted total pressure is simply given by the sum of the vapor pressure and the gas (air pad) pressure. Assuming ideal gas behavior and negligible solubility

$$P_g = \frac{m_g RT}{M_g(V - V_l)} \tag{11}$$

where the liquid compression adequately accounts for the gas partial pressure. Figure 5 shows that the total pressure prediction is in reasonable agreement with the data. Two values of Flory's parameter were tried, namely 0 and 0.35. Below 250°C or about 60% conversion, both values yield nearly identical results. At higher conversions, these predictions begin to diverge. The prediction using a χ value of zero is closer to the data although the final pressure is still overestimated by about 50 psi.

Also in Fig. 5, the partial vapor pressure data were reduced by simply subtracting the gas partial pressure from the total pressure. Since liquid density data are usually not available, the pressure is corrected only due to the temperature change (note that this is less accurate than using eqn. (11)) i.e.

$$P_g = P_g^0(T/T^0) \tag{12}$$

Here P_g^0 and T^0 were taken to be 14.5 psi and 15°C, respectively. The results shown in Fig. 5 are in fairly good agreement with the predicted vapor pressure. The discrepancies at the lower temperatures are due to underestimating P_g in eqn. (12) as a result of liquid expansion in the sample. Again, near the end point, the predicted pressure based on a χ value of zero is closer to the data, but is still too high by about 50 psi. The cause for this discrepancy is unknown and is the subject of further investigation.

Finally, the pressure rate data in Fig. 4 are in good agreement with the prediction which is based on the predicted self-heat rate together with eqns. (9) and (10).

Di-t-butyl peroxide

Thermal decomposition of di-t-butyl peroxide has been most extensively studied because of its simple first-order kinetic behavior. The runaway reaction behavior was studied in the present apparatus using an initial charge of 10 g of peroxide and 30 g of toluene. This yields a ϕ-factor of approximately 1.11. For this test the test cell was evacuated prior to charging the sample. The exotherm was first detected at 118°C with an initial self-heat rate of about 0.1°C min^{-1}. Figure 7 shows that a peak rate of 400°C min^{-1} was measured at 235°C and that the reaction terminated quite abruptly at 247.5°C. Using a best-estimate specific heat of 0.505 cal/g°C * for the mixture, the heat of decomposition is calculated to be

$$\Delta H_r = -\frac{\phi c_v (T_{max} - T_0)}{(m/m_t)} = -\frac{(1.11)(0.505 \text{ cal/g°C})(247.5 - 118\text{°C})}{(0.25)}$$

$$= -290 \text{ cal/g}$$

or −42.4 kcal/g-mole. This compares well with the reported value of 43 kcal/g-mole using the ARC apparatus [3]. However, these values are considerably higher than the literature values of 36–37 kcal/g-mole [18–20] which were obtained from bond dissociation energy considerations. The discrepancy is most likely due to the many additional side reactions possible as shall be discussed later. Figure 7 also shows that the initial slope of the self-heat rate data is consistent with the activation energy of 37.8 kcal/g-mole reported in isothermal kinetic studies carried out in the gaseous phase [21].

Figure 8 shows that prior to exotherm onset, the measured pressure was in

* Assumes mixture c_v can be approximated by toluene c_v values. Furthermore, for $c_v \simeq c_p$, the integrated value for c_p is estimated to be 0.505 cal/g°C for the temperature range of 118°C to 248°C [17]. A mean value of 0.5 cal/g°C was used in evaluating ΔH_r in ref. 3.

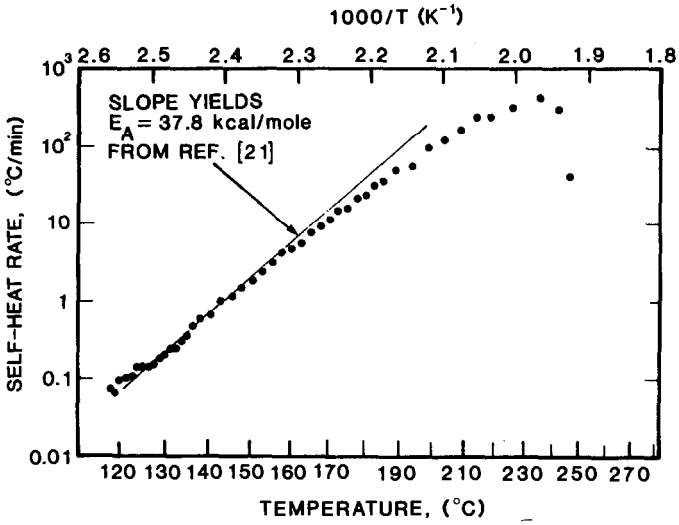

Fig. 7. Self-heat rate data from di-t-butyl peroxide decomposition.

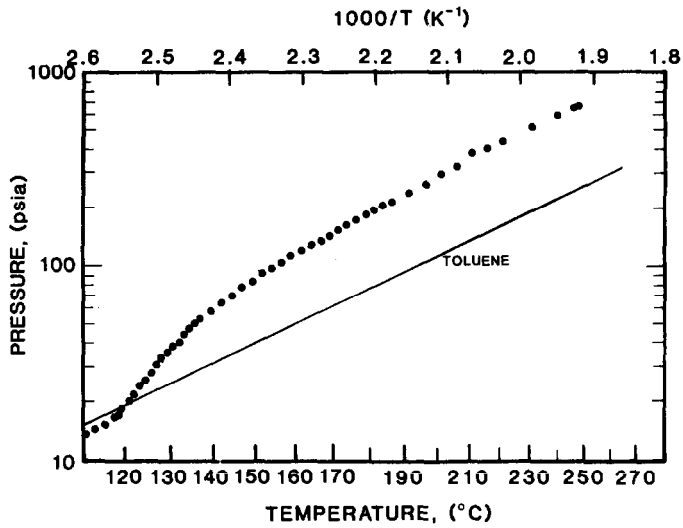

Fig. 8. Pressure–temperature data from di-t-butyl peroxide decomposition.

close agreement with toluene vapor pressure *. However, at the exotherm onset, a much quicker rise in pressure with temperature is observed which is characteristic of decomposition reactions with evolution of gaseous products.

In order to predict the pressure behavior, one must start with the reaction

* Toluene and di-t-butyl peroxide have nearly the same normal boiling point, namely 110.6°C and 111.1°C, respectively.

stoichiometry. Decomposition of di-t-butyl peroxide occurs mainly by the following mechanism in the gaseous phase [20,21]

$$(CH_3)_3COOC(CH_3)_3 \rightarrow 2(CH_3)_3CO\cdot \quad (13a)$$

$$(CH_3)_3CO\cdot \rightarrow (CH_3)_2CO + CH_3\cdot \quad (13b)$$

$$2CH_3\cdot \rightarrow C_2H_6 \quad (13c)$$

so that 1 mole of peroxide would yield 1 mole of ethane. However, in a solvent with an abstractable hydrogen (such as is the case for toluene), the decomposition is more complex. In addition to the products formed by the above mechanism, t-butyl alcohol and other products are formed [20–24]

$$(CH_3)_3CO\cdot + RH \rightarrow (CH_3)_3COH + R\cdot \quad (14a)$$

$$2R\cdot \rightarrow R_2 \quad (14b)$$

$$R\cdot + CH_3\cdot \rightarrow RCH_3 \quad (14c)$$

The subsequent reaction of the t-butoxy radicals and their relative stability in various solvent media determines the number of moles of gas formed. The percentage of these secondary reactions is difficult to estimate without a detailed analysis of the final gas and liquid samples. Such an analysis was not pursued in this study and the pressure–temperature prediction (basically a vapor–liquid equilibrium calculation) has not been attempted.

Despite the various possible side reactions, the rate-determining step is the decomposition of the peroxide into its radicals, eqn. (13a), and hence the overall rate constant should be independent of the solvents present. If the recombination of t-butoxy radicals to reform the peroxide is assumed to require no activation energy, then the activation energy of the rate-determin-

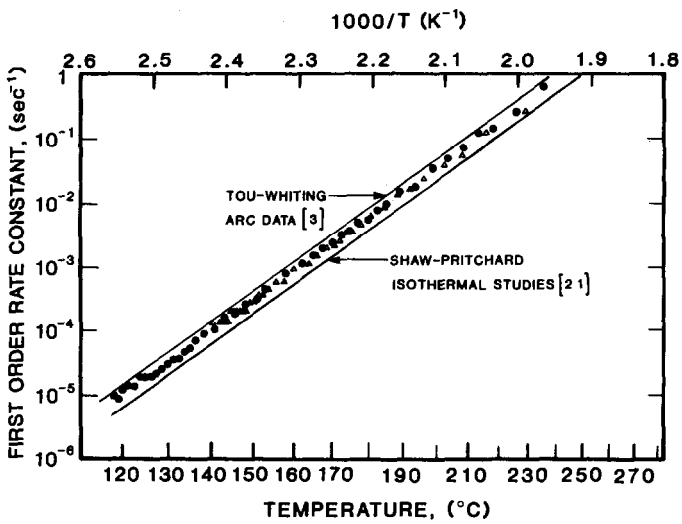

Fig. 9. First-order kinetic rate data from di-t-butyl peroxide decomposition.

TABLE 1

Summary of Arrhenius parameters in di-t-butyl peroxide studies

Source	Type	E_A (kcal mol^{-1})	$\log_{10}A$ (s^{-1})
This study	Runaway in liquid phase	37.71	15.95
Tou–Whiting [3]	ARC runaway in liquid phase	37.80	16.15
Shaw–Pritchard [21]	Isothermal in gas phase	37.78	15.80

ing step is equal to the bond dissociation energy of the peroxide. Indeed the bond dissociation energy has been determined to be 36–37 kcal/g-mole which is in good agreement with the activation energy found from Fig. 7. Figure 9 is an Arrhenius plot of the first-order rate-constant data, illustrating a linear behavior; also shown is another set of data (triangles) obtained using ethylbenzene as solvent instead of toluene. These two sets of data are in good agreement with each other. Table 1 summarizes the Arrhenius parameters, A and E_A, obtained by linear regression of these two sets of data and shows that the current values are in close agreement with those obtained using the ARC apparatus [3] and isothermal studies [21]. Figure 9 shows that the current data are in fact bounded quite closely by the ARC data on the high side and the isothermal data on the low side.

Phenol–formaldehyde reaction

The phenol–formaldehyde base-catalyzed reaction was studied in a runaway situation using the following mixture: 89.9% phenol: 22 g—(0.208 g-mole); 37% formaldehyde–H_2O: 55 g—(0.678 g-mole formaldehyde); 50% NaOH: 2.7 g—(420×10^{-6} g-mole/g-mixture). This yields a phenol–formaldehyde mole ratio of 1 : 3.2 and a ϕ-factor of 1.04 for the apparatus. The reagents were mixed at room temperature before moving to the test cell. The sample was heated up slowly in the presence of pad air and self-heating was detected at 40°C with an initial rate of 0.2°C min^{-1}. The self-heat rate data in Fig. 10 suggest only a single exotherm with a total temperature rise of 120°C. From a reaction chemistry viewpoint, phenol reacts with formaldehyde by addition to give a phenol alcohol and by condensation to form a methylene-bridged compound which can be a linear or a cross-linked polymer [25]. Both reactions are exothermic, yielding between 4.1–5.0 kcal/g-mole for the addition reaction and between 17.7–22.7 kcal/g-mole for the condensation reaction [26,27]. According to ref. 26, the methylol group is unstable in a runaway exotherm situation and the reaction will favor the condensation reaction liberating approximately 21.7 kcal/g-mole (723 cal/g) of formaldehyde. Thus if the reaction proceeds by condensation to form

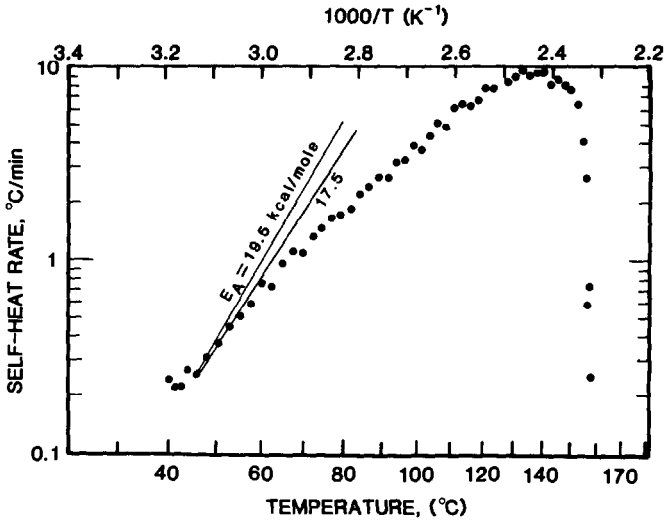

Fig. 10. Self-heat rate data from base-catalyzed phenol–formaldehyde reaction.

linear polymer only, then the calculated temperature rise should be

$$\Delta T = -\frac{\Delta H_r}{\phi c_v}\left(\frac{m}{m_t}\right) = -\frac{(-723\ \text{cal/g})(0.208)(30)}{(1.04)(0.7\ \text{cal/g°C})(79.7)} = 78°\text{C}$$

Here the limiting reactant mass is given by the moles of phenol available multiplied by the molecular weight of formaldehyde (MW = 30) and the average specific heat is estimated to be 0.7 cal/g°C *. Hence this only accounts for 65% of the observed temperature rise. Obviously some degree of cross-linking was present (formaldehyde can be added to phenol in the *ortho* and *para* positions) particularly when formaldehyde was in excess. However, a detailed account of the reaction step is beyond the scope of this study. As for the comparison of the initial slope with the activation energy E_A of 17.5–19.5 kcal/g-mole reported in the literature [26,27], the results shown in Fig. 10 are inconclusive due partly to some data scatter. This again suggests that the reactions are far more complex than could be modeled by simple kinetics alone.

Finally, the pressure data as shown in Fig. 11 can be well correlated by the combined effect of water-vapor and pad gas pressure. The latter contribution was evaluated according to eqn. (12). The finding that the vapor pressure above a phenol–formaldehyde reacting mixture can be approxi-

* For phenol c_v is 0.54 cal/g°C [17], for 37% formaldehyde solution c_v is 0.8 cal/g°C [28], for phenolic resin c_v assumes a mean value of 0.4 cal/g°C [29]; $c_v = 0.75$ cal/g°C for initial mix; $c_v \approx 0.65$ cal/g°C for product mix.

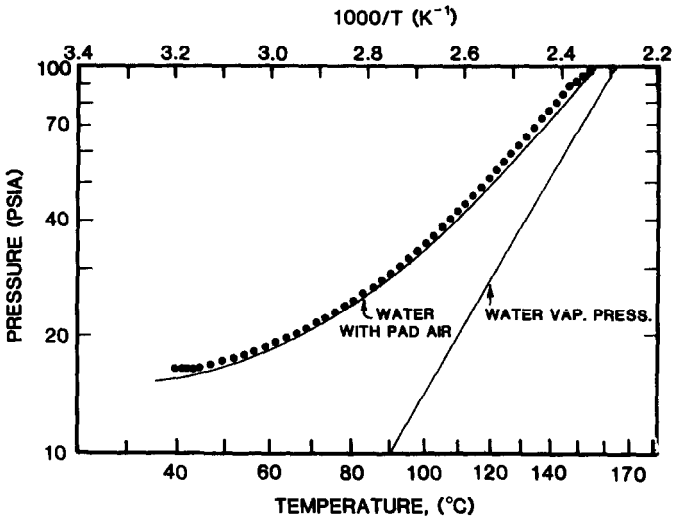

Fig. 11. Pressure–temperature data from base-catalyzed phenol–formaldehyde reaction.

mated by the water-vapor pressure alone is in agreement with earlier studies [26,27].

CONCLUSION

An apparatus with low thermal inertia (typically $\phi \simeq 1.05$) has been developed which produces reliable thermal data in a runaway situation. Data obtained for styrene thermally-initiated polymerization and di-t-butyl peroxide decomposition are in excellent agreement with the kinetic models available in the open literature. The phenol–formaldehyde reaction was well-behaved although no simple kinetic model has been found to describe this reaction, while the pressure data were correlated closely by the water vapor pressure.

APPENDIX A

Styrene–ethylbenzene–polystyrene system data

The physical property equations presented here are taken from ref. 15

Heat of polymerization at 25°C [11] $= -69800$ kJ kg-mol^{-1}

$= -670$ kJ kg^{-1} (160.2 cal g^{-1})

For other temperatures

$$\Delta H_r(T) = \Delta H_r(298.2\ \mathrm{K}) + \int_{298.2}^{T} \left[(C_p)_{\mathrm{polymer}} - (C_p)_{\mathrm{monomer}} \right] \mathrm{d}T$$

Thermally-initiated third-order polymerization model of Hui and Hamielec [13]

$$-\mathrm{d}m/\mathrm{d}t = A[m]^{3/2}m$$

$$A = A_0 \exp(A_1 S + A_2 S^2 + A_3 S^3)$$

$$A_0 = 1.964 \times 10^5 \exp(-10040/T)$$

$$A_1 = 2.57 - 5.05 \times 10^{-3} T$$

$$A_2 = 9.56 - 1.76 \times 10^{-2} T$$

$$A_3 = -3.03 + 7.85 \times 10^{-3} T$$

where m is the amount of styrene monomer, $[m]$ is the styrene monomer concentration in kmol m^{-3}, and S is the mass fraction of polymer.

Vapor pressure

Styrene

$$\ln P^0(\mathrm{N\ m^{-2}}) = 144.02929 - 9630.666/T - 19.36771 \ln T + 0.01775372\ T$$

Ethylbenzene

$$\ln P^0(\mathrm{N\ m^{-2}}) = 88.88045 - 7716.472/T - 9.8965206 \ln T + 6.0871529 \times 10^{-6} T^2$$

Mixture rules

The partial pressure and styrene and ethylbenzene over polymer solution is estimated from the Flory–Huggins equation [16]

$$P_i = \Phi_i P_i^0 \exp[\Phi_p(1 + \chi\Phi_p)]$$

TABLE 2

Liquid-phase density and specific heat data ρ or $C_p = C_o + C_1 T + C_2 T^2 + C_3 T^3$ (T in K)

	C_o	$C_1 \times 10^3$	$C_2 \times 10^6$	$C_3 \times 10^9$
ρ (kg m^{-3})				
Styrene [a]	1209.8	1343.5	1557	−1726
Ethylbenzene	1210.9	−1721.9	2780	−3094
Polymer	1250.1	−605.0	0	0
C_p (kJ/kg K)				
Styrene	2.954	−13.26	39.75	−29.76
Ethylbenzene	1.595	−2.899	13.98	−8.36
Polymer	0.945	2.4	0	0

[a] This curve fit covers a wider temperature range than the equation used in ref. 13. However, it does duplicate closely the values in ref. 13.

The mixture liquid specific volume and specific heat are evaluated based on the additive-value mixing rule, i.e.,

$$v_{mix} = \Sigma(x_i v_i)$$

$$(C_p)_{mix} = \Sigma(x_i C_{pi})$$

Liquid-phase density and specific heat

These data are given in Table 2 as polynomial equations.

Nomenclature

a	activity
A	pre-exponential frequency factor
c_p	specific heat at constant pressure
c_v	specific heat at constant volume
E_A	activation energy
ΔH_r	heat of reaction
k	reaction rate constant
m	mass of limiting reactant corresponding to zero conversion
m_g	mass of gas
m_t	total mass of reacting mixture
M	molecular weight
P	pressure
R	gas constant
t	time
T	temperature
v	specific volume
V	sample container volume
V_l	liquid volume
x	conversion
x_i	mass fraction of component i
ϕ	phi-factor or thermal inertia as defined in eqn. (1)
Φ_i	volume fraction of component i
Φ_p	volume fraction of polymer
χ	Flory parameter
ρ	density

Subscripts

b	bomb or container
g	gas
o	initial or onset
p	polymer

s sample
t total
v volatile vapor
max maximum

REFERENCES

1 A.A. Duswalt, Thermochim. Acta, 8 (1974) 57.
2 D.I. Townsend and J.C. Tou, Thermochim. Acta, 37 (1980) 1.
3 J.C. Tou and L.F. Whiting, Thermochim. Acta, 48 (1981) 21.
4 L.F. Whiting and J.C. Tou, J. Therm. Anal., 24 (1982) 111.
5 W.J. Fenlon, Plant/Operations Progr., 3(4) (1984) 197.
6 J.E. Huff, Plant/Operations Progr., 1(4) (1982) 211.
7 E.S. DeHaven, Plant/Operations Progr., 2(1) (1983) 21.
8 H.K. Fauske and J.C. Leung, Chem. Eng. Progr., 81(8) (1985) 39.
9 Bench Scale ERS Sizing Tools: Equipment Details, Test Procedures, and Illustrations, Fauske & Associates, Inc. Rep. No. FAI/84-4, revised, 1984.
10 J.M. Smith, Chemical Engineering Kinetics, 2nd edn., McGraw-Hill, New York, 1970, Chap. 5.
11 D.R. Stull, in R.H. Boundy and R.F. Boyer (Eds.), Styrene—Its Polymers, Copolymers and Derivatives, Hafner, New York, 1952, Chap. 3.
12 E. Diss, H. Karam and C. Jones, Chem. Eng., 68(19) (1961) 187.
13 A.W. Hui and A.E. Hamielec, J. Appl. Polym. Sci., 16 (1972) 749.
14 A. Husain and A.E. Hamielec, J. Appl. Polym. Sci., 22 (1978) 1207.
15 J.E. Huff, Personal communication, 1981, portions published in ref. 6.
16 S.M. Walas, Phase Equilibria in Chemical Engineering, Butterworth, London, 1985, Chap. 9, pp. 446–448, 456.
17 C.L. Yaws, Physical Properties: A Guide to the Physical, Thermodynamic and Transport Properties of Industrially Important Chemical Compounds, McGraw-Hill, New York, 1977.
18 E.S. Huyser and C.J. Bredeweg, J. Am. Chem. Soc., 86 (1964) 2401.
19 W.A. Pryor, Free Radicals, McGraw-Hill, New York, 1966.
20 S.W. Benson, The Foundations of Chemical Kinetics, McGraw-Hill, New York, 1960, pp. 363–370.
21 D.H. Shaw and H.O. Pritchard, Can. J. Chem., 46 (1968) 2721.
22 J. Murawski, J.S. Roberts and M. Szwarc, J. Chem. Phys., 19(6) (1951) 698.
23 A.L. Williams, E.A. Oberright and J.W. Brooks, J. Am. Chem. Soc., 78 (1956) 1190.
24 A.V. Tobolsky and R.B. Mesrobian, Organic Peroxides, Interscience, New York, 1954.
25 F.W. Billmeyer, Jr., Textbook of Polymer Science, Interscience, New York, 1962.
26 A.D. Booth, M. Karmarkar, K. Knight and R.C.L. Potter, Trans. Inst. Chem. Eng., 58 (1980) 75.
27 P.A. Waitkus and G.R. Griffiths, Saf. Health Plast., Natl. Tech. Conf., Soc. Plast. Eng., 1977, pp. 181–186.
28 J.F. Walker, Formaldehyde, 3rd edn., Krieger, New York, 1975.
29 Modern Plastics Encyclopedia, Vol. 52, 10A, 1975.